

Quantum Hardware Roofline: Evaluating the Impact of Gate Expressivity on Quantum Processor Design

Justin Kallor¹, Mathias Weiden¹, Ed Younis², John Kubiatowicz¹, Bert De Jong², and Costin Iancu²

¹Department of Electrical Engineering and Computer Science, University of California, Berkeley
{*jkallor3, mtweiden, kubitron*}@cs.berkeley.edu

²Computational Research Division, Lawrence Berkeley National Laboratory
{*edyounis, wadejong, cciancu*}@lbl.gov

Abstract—

The design space of current quantum computers is expansive with no obvious winning solution. This leaves practitioners with a clear question: “What is the optimal system configuration to run an algorithm?”. This paper explores hardware design trade-offs across NISQ systems to guide algorithm and hardware design choices. The evaluation is driven by algorithmic workloads and algorithm fidelity models which capture architectural features such as gate expressivity, fidelity, and crosstalk. We also argue that the criteria for gate design and selection should be extended from maximizing average fidelity to a more comprehensive approach that takes into account the gate expressivity with respect to algorithmic structures. We consider native entangling gates (CNOT, ECR, CZ, ZZ, XX, Sycamore, \sqrt{i} SWAP), proposed gates (B Gate, $\sqrt[4]{\text{CNOT}}$, $\sqrt[8]{\text{CNOT}}$), as well as parameterized gates (FSim, XY). Our methodology is driven by a custom synthesis driven circuit compilation workflow, which is able to produce minimal circuit representations for a given system configuration. By providing a method to evaluate the suitability of algorithms for hardware platforms, this work emphasizes the importance of hardware-software co-design for quantum computing.

I. INTRODUCTION

Quantum computers offer an exciting opportunity to explore problems previously considered intractable. An assortment of companies have introduced gate-based quantum machines that range in qubit technology: superconducting transmon qubits [5], fluxonium qubits [4], trapped-ion qubits [10], neutral atoms [20], and several others.

While existing hardware offerings are not mature enough to provide realistic quantum advantage [1] or quantum utility [21], they can be used as a good indicator of the future. Practical questions have already arisen in the community related to the comparison of different hardware solutions: “What computer should I use to run my algorithm? How can I improve my current quantum processor? What gates should I provide to end-users?”

In the current Noisy Intermediate Scale Quantum (NISQ) computing era, gates are imperfect and introduce error in program outputs. Thus, the most important performance metric for current systems is their ability to execute algorithms with the least amount of error, i.e. maximize algorithmic fidelity.

To this end, hardware designers attempt to improve the accuracy of an algorithm’s execution using a multi-stage design process aimed at optimizing behavior across multiple

hardware characterization criteria: gate fidelity, crosstalk (gate parallelism and qubit connectivity), etc. This process, centered around gate fidelity, proceeds as follows: First choose a native entangling two-qubit gate that can be implemented with high fidelity, and that is “good enough” to represent any two qubit process (unitary). After this, develop additional techniques, e.g. crosstalk mitigation, to further improve gate fidelity.

We believe that this design process can be improved upon from both a hardware and end-user perspective. Most hardware characterization metrics ([12], [22], [27]) are gate and algorithm agnostic; therefore, these widely accepted metrics (e.g. gate fidelity) are hard to correlate directly with algorithm performance across systems with distinct hardware characteristics. Full algorithm fidelity models that capture hardware characteristics (gate fidelity and parallelism/crosstalk) have been introduced in the literature [9]. While they are able to assess the fidelity of an algorithm when executed on a single hardware configuration, these models still lack predictive power when varying architectural parameters. The problem stems from the fact that these metrics combine algorithm-agnostic hardware characterization metrics with metrics that characterize the program implementation and resource consumption (e.g. gate count, circuit depth), and implicitly the impact of the program generators and compilers.

In this paper we argue that gate set design should be driven by representational power in the context of a given algorithm or algorithmic workload. In order to attain the most resource efficient implementation, we use custom compilation workflows that combine traditional compilers, such as Cirq [14] or Tket [41], with circuit synthesis tools. Note that the inferences made in this paper could not be obtained without leveraging the BQSKit [45] circuit synthesis tools.

The evaluation is driven by a workload that contains several algorithms of wide interest, such as QFT, QAOA [16], TFIM models [40], Quantum Finance algorithms [17], and Quantum Machine Learning models [8]. For each algorithm we consider problem instances of increasing scale (qubit count) and generate the most resource efficient implementation for a given hardware configuration (gate set and qubit interconnect topology). We consider native entangling gates (CNOT, ECR, CZ, ZZ, XX, Sycamore, \sqrt{i} SWAP), proposed gates (B Gate, $\sqrt[4]{\text{CNOT}}$, $\sqrt[8]{\text{CNOT}}$), as well as parameterized gates (FSim,

XY), together with several qubit interconnect topologies.

This paper makes the following contributions:

First, we introduce analytical models that combine hardware (gate fidelity, parallelism and qubit connectivity) and algorithm implementation (gate count, depth) characteristics to provide useful guidance for hardware and compiler designers, as well as system end-users. We introduce a comparative performance *roofline* based approach which is able to derive which particular metric can lead to overall improvements in algorithmic fidelity, as well as upper bounds on these metrics past which no additional end-user gains can be expected. For example, when comparing Sycamore (Google) and CNOT (IBM) entangling gates for a particular algorithmic workload, our analyses show that there are ranges of relative gate fidelities where one configuration can always outperform the other. Once a certain *threshold* fidelity has been attained, no improvements in one- or two-qubit gate fidelity on any architecture can lead to better relative performance with respect to the other.

Next, we introduce a circuit synthesis based compilation procedure which indicates that the existing gate set design criteria that favors choosing gates based on their attainable fidelity and representational power of random two-qubit process may be misleading. Instead, our analysis shows that the criteria should be augmented with their representational power for multi-qubit processes (e.g. three qubit) that are drawn from implementations of existing algorithms. For example, while the B-gate [46] is the most expressive gate for two qubit unitaries, we cannot uncover advantages when using it to represent complex programs. When compared against CNOT, B-gates lead to gate count increases and possible fidelity decreases. At the other end of the spectrum, we show that several low-entanglement gates such as $\sqrt[4]{\text{CNOT}}$ and $\sqrt{i\text{SWAP}}$ are sometime able to offer similar expressive performance as maximally entangling gates for important circuits such as TFIM, QFT, and QAE, leading to better algorithmic fidelity.

As discussed in Section IX, we believe our assessment procedure extends well beyond NISQ into the Fault Tolerant era of quantum computing.

II. QUANTUM HARDWARE CHARACTERIZATION AND BENCHMARKING

Today’s systems are dominated by superconducting (IBM, Google) and trapped ion (Quantinuum, IonQ) qubits. Neutral Atom (QuEra, Atom Computing) and silicon-spin qubits (Intel) are starting to gain traction, and several other technologies are being developed. All these systems expose to end-users a universal gate set [32], composed of single-qubit and entangling two-qubit native gates. These gate-set choices are outlined in Table I. Several methods exist to characterize today’s quantum machines:

Average Gate Fidelity: The widest used characterization and processor optimization metric is the *average gate fidelity*, which captures the probability that a state does not succumb to any error when a gate is applied. Fidelity can be measured using Randomized Benchmarking (RB) protocols [22], [27], [28], which use random Clifford gates to create an identity

channel over a set of qubits. Averaged over a randomized group of these Clifford circuits, the error of the quantum channel simplifies to a depolarization channel with a single probability p , the average infidelity of the gate’s application. By using variable lengths of random Clifford circuits, existing protocols calculate the infidelity per gate (p_{gate}): fidelity is then computed as $1 - p_{\text{gate}}$.

In 2019, Google introduced the cross entropy benchmarking (XEB) protocol [2] as another way to compute average gate fidelity. Importantly, this study also shows that the total average fidelity of a circuit can be approximated using a simple *digital error model*, validated for NISQ size systems:

$$\mathbf{F}_d = \prod_{i=1,2} f_i^{n_i}$$

where n_i is the number of i -qubit gates in the circuit, and f_i is the average fidelity of an i -qubit gate.

As RB protocols have trouble scaling past three qubit processes, Cycle Benchmarking (CB) [15] has been proposed to improve characterization scalability to larger processes (and hardware). CB based protocols indicate that besides average gate fidelity, hardware dependent metrics such as qubit connectivity and algorithm specific metrics such as gate parallelism per cycle need to be taken into account when assessing algorithm fidelity.

Quantum Volume: Quantum Volume (QV) [12] characterizes the capability of hardware to execute random circuits of a certain size. This metric cannot be used to compare the fidelity of different process implementations running on the same machine or that of a single process running across different machines.

Algorithmic Qubits: IonQ’s Algorithmic Qubits (AQ) metric [9] captures a system’s ability to execute an algorithmic workload. AQ protocols measure the largest number of effectively perfect qubits you can deploy for a typical quantum program. It is similar to QV, but it additionally considers quantum error correction and presents a clear and direct relationship to qubit count. The AQ metric captures the impact of the compilation tool-chain.

All of these protocols and metrics reveal different useful information about a single configuration of quantum machine. However, they all fail when comparing across different hardware and gate sets. While we can measure the fidelity and quantum volume of a CNOT-based machine and of a Sycamore-based machine, this does not give us any information on their respective abilities to run a given algorithm. AQ encapsulates the algorithmic potential of different hardware, but it is still unable to quantify the degree to which one needs make changes to an architecture’s configuration in order to provide better comparative performance.

In order to make these inferences, we advocate for an algorithmic workload based approach centered around circuit fidelity models that combine hardware characterization metrics with the hardware’s ability to represent and implement a particular algorithm. We start with the simple digital model based on average gate fidelity, which we then extend to

Hardware	# Qubits	Technology	Connectivity	Gate Set	1Q/2Q Error(RB/XEB)
Google Sycamore	54	Superconducting	Mesh	1Q: XZ, RZ 2Q:FSim, \sqrt{i} SWAP, Sycamore, CZ	0.001 / 0.01
IBM Eagle r3	127	Superconducting	Mesh	1Q: SX, RZ, X 2Q: ECR	0.0002 / 0.007
IBM Hummingbird r3	65	Superconducting	Mesh	1Q: RZ, SX, X 2Q: CNOT	0.00027/ 0.012
IBM Falcon r5	27	Superconducting	Mesh	1Q: RZ, SX, X 2Q: CNOT	0.0003/ 0.0079
Rigetti Aspen M3	79	Superconducting	Mesh	1Q: RX, RZ 2q: CZ, XY	0.001/ 0.14, 0.092
Quantinuum H2	32	Ion Trap	A2A	1Q: U1, RZ 2Q: ZZ	3e-5/0.002
IonQ Forte (2024)	35	Ion Trap	A2A	1Q: GPI, 2Q: ZZ, XX	0.0002/ 0.0040
IonQ Aria	21	Ion Trap	A2A	1Q: GPI, 2Q: XX	0.0006/ 0.0040

TABLE I: Summary of existing commercial Quantum Computing hardware [3], [14], [19], [35], [38]. As we can see, most devices available now are superconducting or ion trap devices, with superconducting devices proving to be easier to scale. This contrasts the ion trap devices which show on average higher RB fidelity. Additionally, superconducting qubits have a mesh (2D Nearest Neighbors) topology while ion traps are all-to-all (A2A).

account for crosstalk due to parallel gate execution as well as qubit connectivity (an idle qubit can be affected when executing an operation on a neighboring qubits).

III. QUANTUM ALGORITHMS AND COMPILERS

The digital model indicates that circuit fidelity is determined by the average gate fidelity and the circuit gate count: improving both metrics will improve algorithmic fidelity. The gate count for a given algorithm implementation is determined by hardware characteristics: 1) representational power of the native gate set; and 2) qubit interconnection topology.

Due to exponentially compounding gate infidelities, the dominant factor in the digital model is gate count. This has two consequences: 1) comparisons between system configurations should be done using the implementation with the fewest number of gates attainable, together with the lowest depth or highest gate parallelism; and 2) the compilation tool-chain plays a very important role in determining the overall “performance” of a given configuration.

A. Quantum Algorithms

Domain generators [30], [35] that produce the circuit associated with a given algorithm tend to have the following common characteristics:

- They are developed to generate circuits in a restricted gate set. Most generators use directly the CNOT gate, while some hardware-vendor-provided generators target only vendor supported native gates. Thus, the compiler’s ability to translate a circuit between gate sets is paramount for accurate architectural comparisons.
- The generated circuits have a logical qubit connectivity that resembles the domain level structure. For example, optimal QFT circuits are generated assuming an all-to-all qubit connectivity. Circuits generated for fermionic [30] interactions map fermions to qubits using a logical topology that resembles the structure of the physical system modeled. Thus, the quality of the routing algorithm within compilers matters for accurate architectural comparisons.
- Some generators are deemed as optimal. Optimality here relates to asymptotic complexity: a good compiler can greatly reduce the constants that appear in the complexity formula. Again, a good quality compiler is paramount.

B. Quantum Compilers

Conceptually, quantum compilers perform several circuit transformation functions: 1) eliminate gates that are redundant

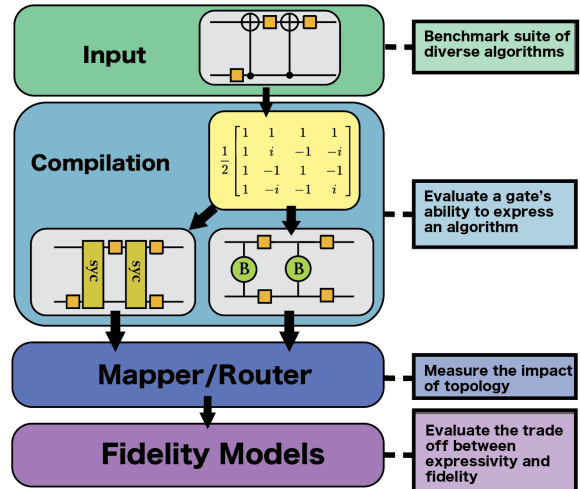


Fig. 1: Our Hardware Comparison Procedure: A synthesis-based cross-compilation process (sometimes called “transpilation”) allows us to explore multiple gate sets and their ability to express an algorithm in terms of gate count, depth, and parallelism. From there, we can understand the effects of topology and fidelity on the overall performance of a quantum machine.

or can be simplified from the circuit; 2) map and route the input circuit to the hardware configuration; and 3) translate (transpile) the input circuit to a different gate set. As seen in Figure 1, compilation forms an important part of our evaluation process.

Traditional vendor compilers use peephole optimizations based on 2-qubit gate synthesis (KAK [42] decomposition), application of gate commutativity rules, or domain specific pattern rewriting rules (e.g. Tket’s phase gadgets [11]). They also provide mapping and routing algorithms [23], [35], [41] and compilation to multiple gate sets (“transpilation”). In particular, transpilation is performed using a one-to-one gate rewriting rule: any two-qubit gate is rewritten directly from one (e.g. CNOT) to another (e.g. Syc).

Circuit synthesis [37], [45] based tools have been introduced recently and have been shown to provide better quality implementations ([13], [26], [43], [44]) when compared against vendor compilers, albeit at the expense of increased compilation time. Some of these tools integrate optimization [13] with mapping [26] and gate transpilation [44]. They can search a large space of circuit structures and transformations. When considering transformations, these tools are able to perform global optimization of multi-qubit circuits, as opposed to peephole pattern replacement and one-one gate translation

Family	Benchmarks (circuit_width)
TFIM	TFIM_16, TFIM_64, TFX_Y_16, TFX_Y_64
QAE	qae_9, qae_13, qae_17, qae_21
QFT	qft_4, qft_12, qft_64
QAOA	qaoa_10
QPE	qpe_14, qpe_18
Adder	adder_9, adder_63, mul_10, mult_60
Shor	shor_12, shor_16, shor_24, shor_28
Grover	grover_5
Hubbard	hubbard_4, hubbard_8, hubbard_12
QML	qml_6, qml_13, qml_22
VQA	vqe_12 (LiH), vqe_14 (BeH ₂)

TABLE II: Our Benchmarks: List of benchmark circuits organized by family. Each circuit was initially created with CNOT and U3 gates.

offered by vendor compilers.

All compilation tools have one thing in common: the compilation workflow is custom and it consists of repeated applications of passes and transformations. While it is hard to quantify the impact of optimization, mapping, and transpilation phases in isolation, we note that compilers can realize up to an order of magnitude in gate count reduction, even when the input circuit is “optimally” generated.

IV. EVALUATION PROCEDURE

We used the algorithms shown in Table II for our evaluation. They include many important categories including Variational Algorithms (VQA and QAOA) [16], [34], Finance (QAE) [17], Number Theory (QFT, QPE, Shor) [6], Physical Simulation (Hubbard, Ising(TFIM)) [7], [40], Search (Grover [29]), and Quantum Machine Learning (QML). The QML circuit is based on [8] and has an n-bit encoder and a two-local network. Most benchmarks were generated using Qiskit circuit generators [35], while the TFIM circuits were generated with F3C++ compiler [33]. All input circuits were generated using CNOT entangling gates, which is standard practice. For each algorithm we generate several instances across inputs and circuit sizes (number of qubits). Overall, we believe that our algorithmic workload provides a good sampling of the space of circuit implementations. We consider up to 64 qubit programs, with gate counts as high as 37000 accounting for a maximum depth of 44500. The logical topology of these programs ranges from linear in TFIM to the all-to-all connectivity in QFT.

We translate and optimize the benchmarks for native gates present in today’s hardware (CNOT, ECR, CZ, ZZ, XX, Sycamore, \sqrt{i} SWAP), as shown in Table I. Additionally, we examine experimental gates theorized to provide algorithmic fidelity advantages due to either high expressivity or high fidelity, B and $\sqrt[4]{\text{CNOT}}$ or $\sqrt[8]{\text{CNOT}}$ respectively.

Figure 1 illustrates our process. We use a custom compilation workflow that composes compilers (Qiskit, Cirq, Tket) with the BQSKit [45] circuit synthesis tools and selects the best circuits that result. Table III shows a sampling of these results. While details of the compilation workflow are beyond the scope of this paper, to our knowledge, we generate the best attainable implementations of a given algorithm on a given

Benchmark	Size	Gate	BQSKit		Tket		Cirq		Qiskit	
mul_10	163		a2a	mesh	a2a	mesh	a2a	mesh	a2a	mesh
		cz	67	89	104	134	134	227	132	141
		b	110	125	208	480	-	-	-	-
		syc	103	139	208	319	260	364	-	-
qft_16	264	cz	237	336	240	522	264	563	264	426
		b	242	302	480	1044	-	-	-	-
		syc	241	365	480	828	288	755	-	-
TFIM_16	240	cz	200	200	240	240	240	240	240	240
		b	200	202	480	480	-	-	-	-
		syc	200	208	480	219	440	440	-	-

TABLE III: Comparison of two qubit gate counts for a subset of the benchmarks and gate sets across our different compilers. The first number under each compiler is for an all-to-all topology system, while the second number is for a mesh topology. Synthesis based compilers, such as BQSKit, produce the circuits with the least amount of gates. Note that Cirq (Qiskit) is unable to compile to the B Gate (B and Sycamore Gate).

hardware configuration. These resource “optimal” circuits¹ are then run through our fidelity models described in Section VI in order to compare overall performance.

V. GATE REPRESENTATIONAL POWER

Given a reference implementation using CNOT gates, in Figure 2 we show the relative two-qubit gate count (averaged across circuit families) after re-targeting to a particular gate. This data shows the ability of a gate to represent a particular algorithm, i.e. it captures its expressivity and entanglement power. When considering existing native gates, the {CZ, ZZ, XX, ECR} set seems to have the same representational power as CNOT gates. The native gates {Sycamore, \sqrt{i} SWAP} have lower representational power than CNOT, as illustrated by their higher gate counts. When considering theorized gates, we see that {B, $\sqrt[4]{\text{CNOT}}$, $\sqrt[8]{\text{CNOT}}$ } have overall lower representational power than CNOT. This is surprising as the motivation behind the introduction of the B-gate was its higher-than-CNOT representational power.

This behavior is also algorithm dependent. The Ising Model, QAE and QFT circuits require almost the same number of gates, irrespective of which gate it is used. For the rest of the circuits, we see more nuanced behavior. The gate set {CZ, ZZ, XX, ECR, CNOT} leads to the least amount of gates used, with much higher gate counts for the set {Sycamore, \sqrt{i} SWAP, B, $\sqrt[4]{\text{CNOT}}$, $\sqrt[8]{\text{CNOT}}$ }.

Assuming that gates have different fidelities, the data indicate that the machine with the highest fidelity will be best suited to execute TFIM, QFT, and QAE. For the rest of the algorithms, suitability needs to be examined while considering both gate fidelity and circuit structure (gate count etc.). Our data also indicates that gate representational power with respect to full algorithms needs to be taken into account when selecting a system configuration. We discuss in detail representational power trade-offs in Section VIII.

VI. CIRCUIT FIDELITY MODELS

In the NISQ era, it is critical to maximize the probability that a circuit’s output state is correct. The output expectation

¹Meaning they do not improve with further compilation and optimization.

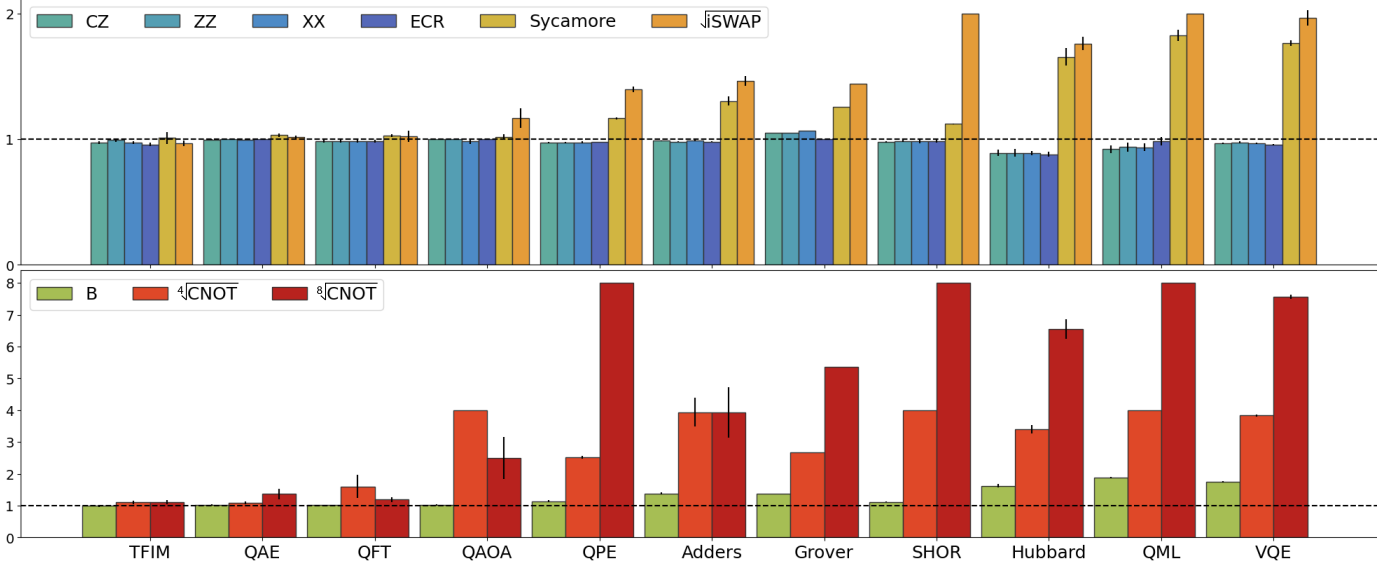


Fig. 2: Normalized two-qubit gate count for existing hardware (top) and theorized hardware (bottom). We plot the relative count with respect to the best attainable CNOT based circuit (best optimization across compilers). This shows the gate count when using the logical algorithm connectivity, which correlates to the gate's respective ability to represent the algorithm.

can be described a function of the average gate fidelity of the machine, written as [32]:

$$\mathbf{F}_{\text{gate}}(\mathcal{E}, U) = \int d\psi \langle \psi | U^\dagger \mathcal{E}(\psi) U | \psi \rangle$$

where U is the target unitary and \mathcal{E} is the erroneous channel trying to implement U .

To assess algorithm fidelity on a particular system configuration, we use a series of models that capture circuit characteristics together with an increasing number of architectural features: (1) gate fidelity; (2) gate fidelity and parallelism. In Section VII-E we discuss a model based on qubit connectivity as well.

Let $\mathbf{F}(\cdot)$ denote a circuit fidelity model, and let A and B denote two distinct system configurations. In order to enable system comparisons, we analyze the *objective function* given by:

$$\pi = \mathbf{F}^A(\cdot) - \mathbf{F}^B(\cdot)$$

A. Gate Fidelity

Our first model is derived from [2], in which the authors verify that the measured fidelity and estimated fidelity based on this model track almost exactly for their tested circuits.

Definition 1 (Digital Fidelity Model). The average circuit fidelity \mathbf{F}_d can be estimated as

$$\mathbf{F}_d = \prod_{i=1,2,\dots} f_i^{n_i}$$

where n_i is the number of i -qubit gates in the circuit, and f_i is the average fidelity of an i -qubit gate. For systems with only one- and two-qubit native gates this becomes:

$$\mathbf{F}_d = f_1^{n_1} \cdot f_2^{n_2}$$

with the objective function:

$$\pi_d = f_1^{A n_1^A} \cdot f_2^{A n_2^A} - f_1^{B n_1^B} \cdot f_2^{B n_2^B}$$

B. Gate Fidelity and Parallelism

Parallel execution impacts (negatively) the attainable gate average fidelity. To capture this, we use a model based on Cycle Benchmarking [15]. The protocol considers circuits as a series of cycles, with which we can calculate a single cycle fidelity as function of the 1-qubit and 2-qubit process fidelities (γ). Note that the process fidelity and average fidelity as defined above are related by the following equation [18]:

$$f = \frac{d \cdot \gamma + 1}{d + 1}$$

where $d = 2^n$ is the dimension of the qubit register with n qubits. We consider the register size of each cycle as the gate parallelism per circuit cycle. We average over the circuit parallelism and compute an average circuit register size.

Definition 2 (Cyclic Fidelity Model).

$$\mathbf{F}_c = \prod (1 - e_i * P_i)^m$$

where P_i is the average parallelism of i -qubit gates in the circuit, and e_i is the average process infidelity for an i qubit gate ($1 - \gamma_i$). e_i can be measured using the Cycle Benchmarking protocol. The objective function for machine comparison becomes:

$$\begin{aligned} \pi_c &= \mathbf{F}_c^A - \mathbf{F}_c^B \\ &= (1 - e_1^A * P_1^A)^{m^A} \cdot (1 - e_2^A * P_2^A)^{m^A} \\ &= (1 - e_1^B * P_1^B)^{m^B} \cdot (1 - e_2^B * P_2^B)^{m^B} \end{aligned}$$

C. Validation

These models trade off accuracy for tractability. While full noise simulation is able to give the most accurate view of algorithmic fidelity, it does not scale to system sizes of interest. However, we can use it as a point of comparison to validate

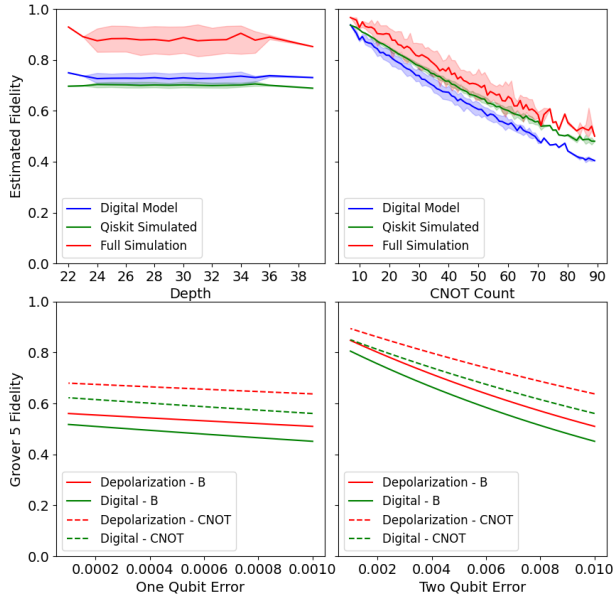


Fig. 3: Validation experiments for our fidelity model. (a) Plot against full simulation on IBM Noisy Simulator and derived depolarization channel. We keep constant depth circuits with varied CNOT count gates. (b) Fidelity plot of constant count circuits as we vary circuit depth. (c) Varying the 1-qubit gate error of our model vs. a general depolarization model. (d) Varying the 2-qubit gate error of our model vs. a general depolarization model.

our models. We focus on validating the digital model for our experiments since that model is directly based on RB/XEB protocols which are available across all of our tested machines.

We first compare our algorithm on random circuits with varied gate count and depth (see Figures 3a, 3b). We compare our digital model against two other models: full simulation and a depolarization channel model. We use Qiskit’s provided noisy backends which account for T1 and T2 coherence times of qubits, as well as explicit error channels for each gate application [35]. We then run the Randomized Benchmarking protocol on this simulator to derive one- and two-qubit fidelities that we use to characterize a depolarization error channel. We expect our model to lower bound both other procedures, which we see in Figures 3a and 3b. Importantly, the trends in all 3 lines are identical as we vary CNOT count and depth.

Secondly, we ensure that our model outputs similar relative results as we vary one- and 2-qubit error for different gate sets. We show these experiments in Figures 3c and 3d for the *grover_5* circuit transpiled to a CNOT machine and a B-gate machine. We see that the conclusions we would draw from either model are the same as we vary the error. We feel that the correlations seen in our model across these experiments in addition to the correlation seen in experiments run by Google on real hardware [2] validate the utility of our fidelity model.

VII. EVALUATING QUANTUM MACHINES

Now, we can finally answer the question “*What machine should I use to run my algorithm?*”.

The answer is rendered trivial when considering currently published gate fidelity figures. Quantinuum boasts by far the highest 2-qubit gate fidelity at 0.998 and its ZZ gate can

express our algorithmic workload well. The H2 systems also provide all-to-all connectivity which requires no additional routing. For algorithms that use more qubits than H2’s capacity, the models suggest the IBM Eagle system.

A more interesting question is how could system configurations be changed in order to improve competitiveness, e.g. : “*How can other machines become better than H2?*”.

A. Quantifying Design Trade-offs

Our procedure allows us to quantify the trade-offs between a gate’s representational power for an algorithm and its fidelity. This is a comparative analysis where we vary the models’ parameters and solve for the objective function as defined in Section VI. As gates continue to improve and calibration/noise-mitigation techniques advance, architects and end-users must consider:

- 1) “How much should I improve my gate fidelity in order to out-perform other machines? How does this vary by algorithm class?”
- 2) “Does single-qubit gate count matter for relative performance? At what point do we no longer care?”
- 3) “Does offering multiple entangling gates help with my machine’s ability to express a circuit? Do parameterized entangling gates such as the FSim or XY gate help? If calibrating a more flexible machine leads to a drop in fidelity, how much drop can we afford?”
- 4) “How much of a fidelity improvement do I need to provide in order to overcome topological features of my machine?”

Given that the maximum attainable gate fidelity is 1, in order to compare NISQ-era devices, we want to use realistic constraints. First, to simplify the model, we will initially limit the single-qubit gate type to only the $U3$ gate. Current machines have parameterizable rotation gates that can be composed to perform any arbitrary single-qubit unitary. As 2-qubit gate errors still dominate, this simplification is justified. Based on Table I, single-qubit gate fidelities vary from around 0.999 to 0.99999 across all quantum machines considered. For 2-qubit gates we range from fidelities of 0.990 to 0.999.

B. Two-Qubit Gates Analysis

We use the *adder_9* algorithm to directly compare IBM Falcon (CNOT) with Google Sycamore (Sycamore) machines as our driving example. The resulting objective function (defined in Section VI) becomes:

$$\pi_d = f_1^{A70} \cdot f_2^{A49} - f_1^{B91} \cdot f_2^{B66}$$

For comparisons, we rewrite the objective function to use the Sycamore fidelity relative to CNOT. We vary the CNOT fidelity along the x-axis and the relative Sycamore fidelity along the y-axis. We then have two remaining free variables:

$$\pi_d = f_1^{A70} \cdot x^{49} - f_1^{B91} \cdot (x \cdot y)^{66}$$

The results are summarized in Figure 4. Each point represents a two-system configuration we are comparing, with

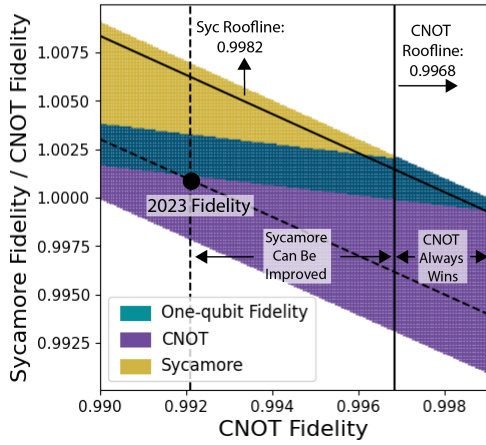


Fig. 4: Machine capability to execute the `adder_9` algorithm. *CNOT* fidelity is on the *x*-axis and the relative Sycamore fidelity on the *y*-axis. We plot the winning machine at each point. The middle area shows where the choice of best machine is a function of the single-qubit fidelity. In the other areas, each machine wins irrespective of 1-qubit gate fidelity. The published 2-qubit gate fidelities are shown with the black dotted lines: interestingly the *CNOT* based system is better, despite the better Sycamore gate fidelity.

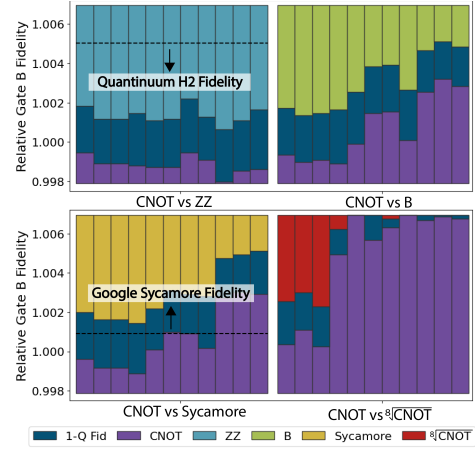


Fig. 5: Gate set comparison against *CNOT*. *CNOT* fidelity fixed to the IBM Falcon. Each configuration can be improved by tuning the 2-qubit gates. Encouragingly, low entanglement gates $\sqrt[3]{CNOT}$ can provide better overall circuit fidelity for some algorithms. The bars correspond to the circuit families: *TFIM*, *QAE*, *QFT*, *QAOA*, *QPE*, *Adders*, *Grover*, *Shor*, *Hubbard*, *QML*, and *VQE*.

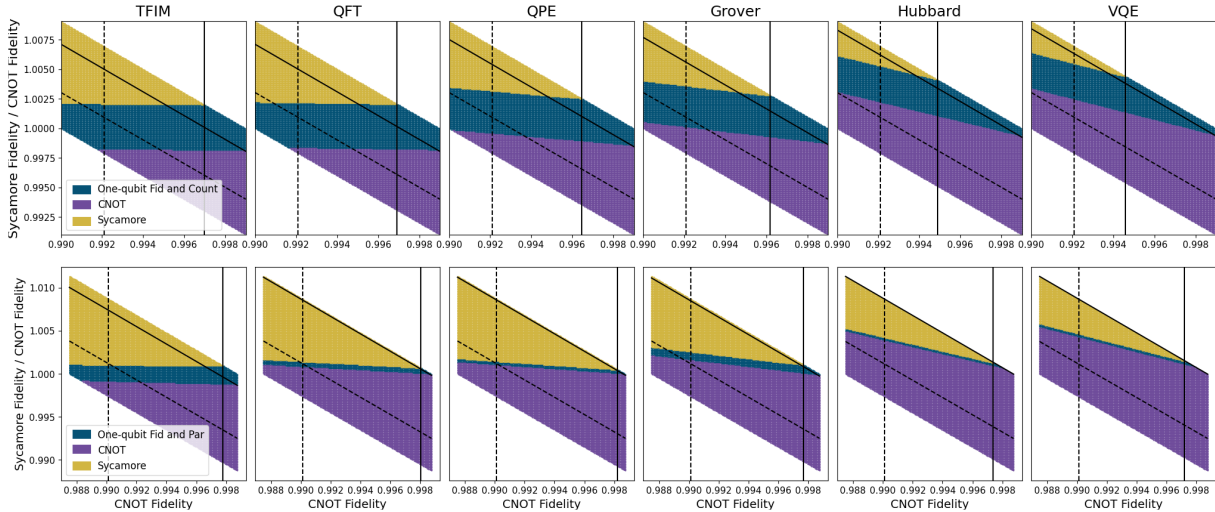


Fig. 6: Comparison of *CNOT* and Sycamore based systems when varying 1-qubit gate fidelity. The black dotted lines show the current NISQ fidelities for the two compared machine (IBM Falcon vs. Google Sycamore). Regions labeled Sycamore and *CNOT* denote which configuration performs best independent of 1-qubit gate fidelity. In the “One-qubit” region, behavior is determined by 1-qubit and 2-qubit gate fidelity.

the 2-qubit fidelities set according to the *x* and *y* position. We identify three behavioral regions. In two regions, one configuration wins against the other, *no matter the single-qubit gate fidelity of the system*. In these regions 2-qubit gate fidelity and expressivity determine system behavior. In the central region, the behavior depends on the fidelity of single-qubit gates: one machine can be improved relative to the other by tuning their single-qubit gate fidelity. For each system we also compute a *2-qubit gate threshold fidelity*, shown with continuous lines: once that is reached on a system, no improvements² in the other system’s 2-qubit gate fidelity will change the overall ordering. We also plot the published fidelities of the respective hardware gates with a dotted line. The distance between actual and threshold fidelity for a gate

indicates a window of opportunity to improve the other system.

We refer to this method of relative comparison as a *quantum hardware roofline*, as it allows us to compute bounds on the required improvements for a particular system configuration. For example, In Figure 4, once the *CNOT* gate reaches the *threshold* fidelity of 0.9968, no improvements in the Sycamore fidelity will outperform a *CNOT* based machine.

Figures 5 and 6 extend these results across algorithm classes and gatesets. Figure 5 compares several gates against the *CNOT* gate whose fidelity is fixed to that of the IBM Falcon system. Again, configurations can be improved by improving only 2-qubit fidelity, or by improving 1-qubit and 2-qubit gate fidelity together. The exact behavior is algorithm and gate set dependent. Encouragingly, low entanglement gates can provide advantages for some algorithms.

²We vary the fidelities within the constraints of our model.

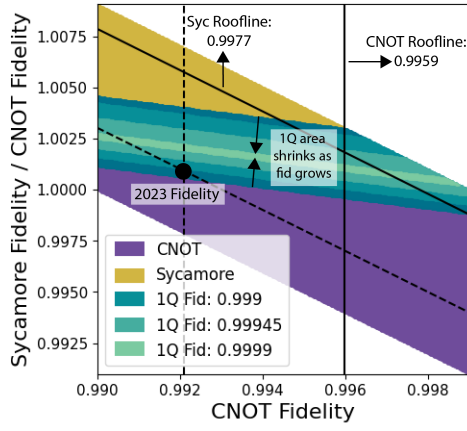


Fig. 7: This plot shows the behavior of the 1-qubit dependent region as we enforce a higher and higher 1-qubit fidelity. For *adder_9*, the region disappears entirely when you reach a 1-qubit fidelity of 0.999988.

Figure 6 shows the circuit fidelity comparison plot for the Digital Model and the Cyclic Model. Both the current behavior and the roofline fidelities for both gates vary greatly with the target algorithm class. The trends are similar across models, with the Cyclic Model placing a much smaller emphasis on the single-qubit configuration. This is to be expected since the model penalizes the impact of 2-qubit gates.

C. Single-Qubit Gate Analysis

The region where machine performance can be improved by tuning 1-qubit gate fidelity is determined by the algorithm gate count together with the actual gate fidelity. To understand the implications for 1-qubit gate design we consider the closure of the behavior across “any” algorithm. Therefore, we consider that the 1-qubit gate count is constrained and related to the two-qubit gate count. Based on our empirical data, we loosely choose the lower bound as $\frac{1}{8}$ of the corresponding 2-qubit gate count. As the upper bound we consider twice the 2-qubit gate count: two consecutive U3 gates can be combined into one, so there is at most two 1-qubit gates in between the 2-qubit gates.

Now, we can allow the 1-qubit gate count to vary in this range and analyze how the objective function behavior changes as we fix single-qubit fidelity (F_1) for both machines.

$$\pi = (F_1)^{n_1^A} \cdot x^{4153} - (F_1)^{n_1^B} \cdot y^{5944}$$

The analysis for *adder_9* on the Falcon and Sycamore machines is shown in Figure 7. The 1-qubit dependent region shrinks as the single-qubit fidelity improves, even if we allow for any single-qubit gate count! At some value, the crossover region completely disappears. We denote this as *single-qubit threshold fidelity*: once this is reached, no improvement in 1-qubit gate fidelity will improve comparative performance between two configurations.

We can solve for the threshold fidelity for different initial 2-qubit gate counts, as present in algorithms. We set up the objective function such that the 2-qubit counts for each

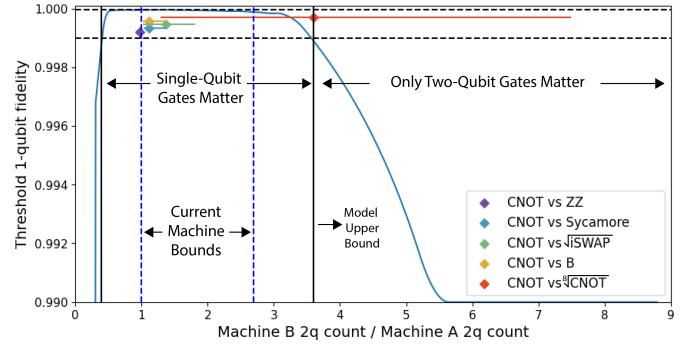


Fig. 8: The X-axis shows the 2-qubit gate count ratio when comparing the implementations on two machines, while the Y-axis shows the resulting threshold 1-qubit fidelity. We also plot the range of 2-qubit gate count ratios we see for each gate compared to CNOT. The black dotted lines show the current NISQ single-qubit fidelity range. When using the upper bound on gate count ratio, the ordering of most machine comparisons is affected by the single-qubit gates. This quickly changes when we consider specific machines as shown in Table IV.

Machine 1	Machine 2	NISQ Threshold Ratio
IBM Falcon	IBM Eagle	1.46
IBM Falcon	Google Sycamore	1.70
IBM Falcon	Quantinuum H2	1.06
IBM Eagle	Google Sycamore	2.69
IBM Eagle	Quantinuum H2	1.69
Google Sycamore	Quantinuum H2	1

TABLE IV: The upper bound on 2-qubit gates ratio that determines the impact of 1-qubit gate tuning for selected pairs of NISQ machines. We use gate fidelity provided by the data-sheets for each machine [14], [35], [36]. Gate count ratios less than the threshold ratio signify circuits where tuning 1-qubit gates can improve the relative performance. For Sycamore vs. H2 (1), the only way to improve relative performance is by improving 2-qubit gate fidelity, while for the Falcon vs. H2 (1.06) there is a slight window of opportunity.

machine are related by a ratio, and we vary this ratio along the x-axis in Figure 8.

$$\pi = y^{n_1^A} \cdot f_2^{A n_2^A} - y^{n_1^B} \cdot f_2^{B n_2^B \cdot x}$$

As shown in Figure 8, there is an upper bound ratio (3.5) where the threshold fidelity drops below the current worst NISQ-era worst single-qubit fidelities! For any two circuits where the 2-qubit gate ratio is higher than the upper bound (3.5), no improvements in 1-qubit gate on any machine can change relative performance. This explains why for several circuit families, the CNOT machine always beats the $\sqrt[8]{\text{CNOT}}$ machine regardless of the single-qubit configuration!

Using this model, we can derive system-specific upper bound ratios which give direct information about the potential of changing relative performance in practice. Here, we plug into the model the actual 2-qubit gate fidelity ranges of the machines and show results in Table IV. As indicated, the actual upper bounds are around 1.6, much lower than the 3.5 absolute threshold. Overall, this data indicates that for most systems, relative performance orderings can be changed by tuning 1-qubit gates, but for cases such as running QML circuits on Falcon and Sycamore machines, the 1-qubit gates do not matter.

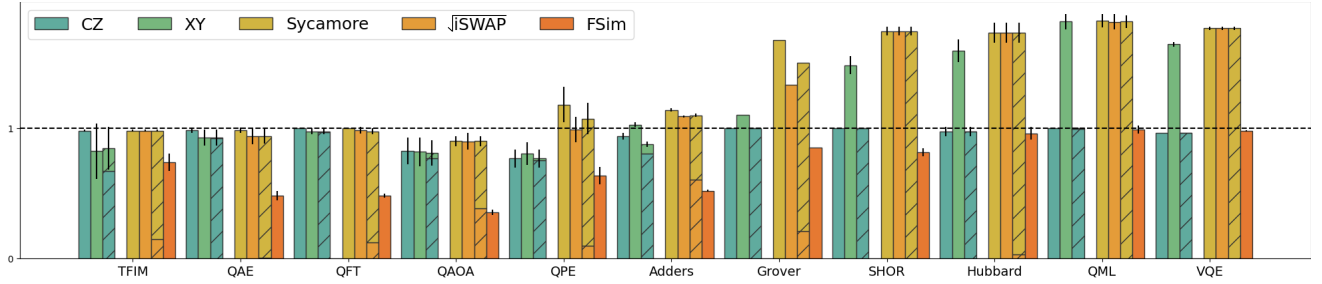


Fig. 9: 2-qubit gate ratios relative to CNOT, for the Aspen and Google hardware systems. We show homogeneous implementations (CZ, Sycamore, \sqrt{i} SWAP), heterogeneous implementations (CZ+XY, Sycamore+ \sqrt{i} SWAP), and parameterized entangling gates (XY, FSim). Heterogeneous implementations (stacked bars) are as good as homogeneous ones. The FSim gate is able to express well all algorithms and it is worth targeting.

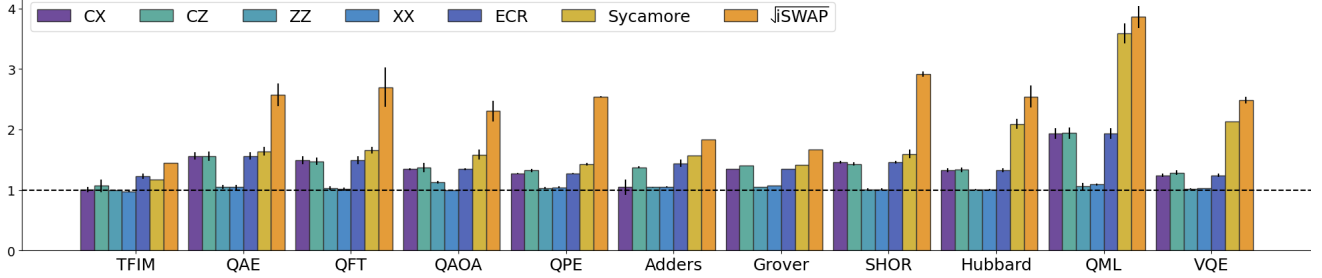


Fig. 10: 2-qubit gate counts averaged across circuit families mapped to each device topology and gate set.

D. Mixing Entangling Gates

Systems such as Aspen and Sycamore offer multiple entangling gates and parameterized entangling gates. These gates will have different average fidelities and may be used together within a single circuit. In Figure 9 we show the 2-qubit gate counts for the Sycamore and Aspen machines when using parameterized and multiple 2-qubit entangling gates within the same circuit. Heterogeneous gate sets Sycamore+ \sqrt{i} SWAP and CZ+XY express circuits as well as the Sycamore or CZ gate alone, respectively. Therefore, on these systems choosing the highest fidelity gate for any algorithm may be sufficient.

The parameterized FSim gate leads to significant gate count reduction when compared to the Sycamore and \sqrt{i} SWAP gates, while the XY Gate provided no benefit over the CZ gate. The FSim gate takes two parameters, while the XY gate only has one. This allows the FSim gate to express complex unitaries more efficiently. Accordingly, FSim implementations can outperform Sycamore gate implementations even with a larger (0.4%) drop in fidelity! The circuit quality of the FSim gate may also point to a finite *spanning gate set* of FSim family gates that are able to express circuits as well as the full parameterized gate. A finite set of constant gates may prove to be easier to calibrate than a fully parameterized gate, leading to a higher gate fidelity.

E. Topology

The physical qubit interconnection topology impacts system behavior by:

- 1) Increasing gate counts when the algorithm logical topology is mismatching, as shown in Figure 10.
- 2) Adding cross talk due to the device qubit couplings.

Architects can use our models to answer: "What fidelity improvement is needed to overcome a more restrictive topol-

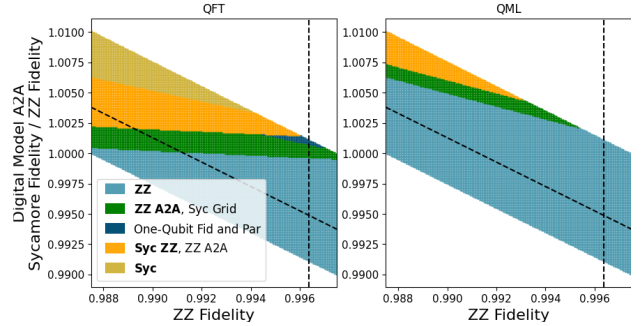


Fig. 11: Topology effects for (ZZ, Sycamore) X (all-to-all, mesh). Dark blue region - relative performance can be changed by tuning 1-qubit fidelity. Light Blue region - ZZ always performs best, regardless of topology. Yellow region - Sycamore always performs best. In the other regions, the bolded configuration performs best.

ogy?". In Figure 11 we compare the capabilities of H2 (ZZ, all-to-all) with Sycamore (Sycamore, mesh) using the cyclic fidelity model. As before, we are able to identify ranges where a certain combination (gate, topology) performs best irrespective of 1-qubit gate fidelity, as well as ranges where relative performance depends on 1-qubit gate fidelity as well. The orange region in the graph shows the fidelity range in which Sycamore loses on account of being mapped to a more restrictive topology. The size of this orange region corresponds to the change in ability to express a circuit, and varies by algorithm.

While Figure 11 is able to model the first effect of topology, we must turn to the coupling-based model introduced in [15] in order to understand cross talk:

$$\mathbf{F}_{\text{c}_{\text{top}}} = (1 - e_{c_1} \cdot C_1)^{n_1} \cdot (1 - e_{c_2} \cdot C_2)^{n_2}$$

where C_i is the number of other qubits on average that

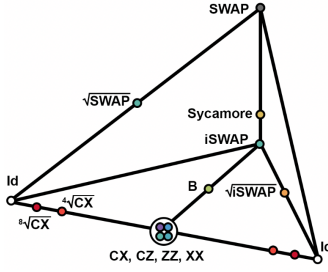


Fig. 12: Projection of various 2-qubit gates onto the Weyl Chamber. Gates located at the same point represent unitaries that differ by single qubit rotations applied to each qubit (a 1:1 mapping).

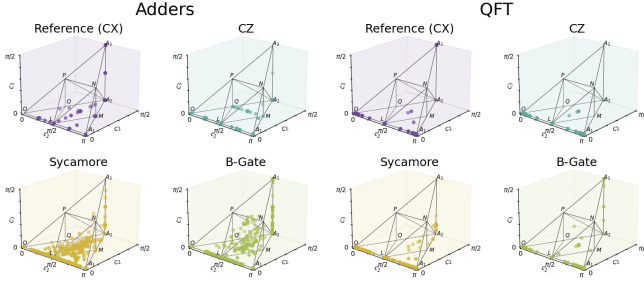


Fig. 13: Position in the Weyl chamber of 2-qubit unitaries/blocks that arise in the Adder group (left) and QFT group (right) for different native gates. The initial spread of Adder unitaries proves to be a very difficult pattern for the Sycamore and B-gates to instantiate, hence the massive increase in gate count. On the other hand, the relatively simple pattern we see in the QFT unitaries (series of controlled rotations) are able to be expressed optimally by Sycamore and B-gates.

each qubit is coupled to and e_{ci} is the error per coupling for an i -qubit gate. C_i is a direct measure of the physical chip topology. For grid topology, usually associated with superconducting qubits, C_2 is a constant between 1 and 4. For all-to-all connectivities provided by ion traps C_2 is instead $\frac{1}{2}N(N-1)$. The error per coupling is measured by the Cycle Benchmarking protocol, but these numbers are not provided for today’s devices.

VIII. EVALUATING GATE REPRESENTATIONAL POWER

A gate set’s ability to realize a circuit comes down to its expressivity and entanglement. Gate *expressivity* identifies a gate’s ability to represent a random two-qubit unitary. Architects often use the Weyl Chamber to directly visualize gate expressivity [25], as shown in Figure 12. The Weyl Chamber removes all local parameters from a 2-qubit unitary and plots it into a tetrahedron. Most 2-qubit gates can express any 2-qubit unitary in three applications (along with single qubit rotation gates). The most expressive gate, the B-gate, can express any unitary in two applications (it can also easily be realized on a superconducting machine) [46].

Gate *entanglement* is a gate’s ability to maximize the entanglement between two qubits. CNOTs and most hardware native gates are maximally entangling, meaning that a single application to two qubits will leave them perfectly correlated. The $\sqrt[4]{\text{CNOT}}$ and $\sqrt[8]{\text{CNOT}}$ gates trade off entangling power for large potential gains in gate fidelity.

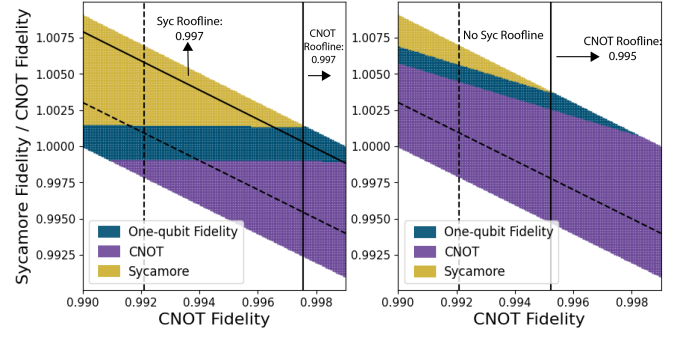


Fig. 14: Comparison of fidelity plots when compiled with synthesis vs. Cirq. Non-local optimization leads to resource-efficient circuits for different gate sets, which results in vastly different comparisons. Note that under the Cirq compilation, there is no Sycamore roofline.

Several trends have become apparent in our research. Most notably, we see that with current state-of-the-art compilation, the B-gate does not lead to better circuits, nor does it increase fidelity. This is surprising, because the B-gate is the most expressive 2-qubit gate. On the other hand, we see some equally surprising positive results for the $\sqrt[4]{\text{CNOT}}$ and $\sqrt[8]{\text{CNOT}}$ gates. These low entangling gates require 4 and 8 applications respectively to represent a single CNOT gate. This makes their comparable expressivity in important circuits such as QFT, TFIM, and QAE circuits exciting.

A. Weyl Chamber Distribution of Two-Qubit Algorithm Blocks

Under our procedure, it is clear that the expressivity and entanglement of a native 2-qubit gate is not strongly correlated with algorithm performance under the currently accepted design criteria. While expressivity is assessed based on the power to implement random 2-qubit unitaries, optimal implementations of algorithms impose structure on the set of 2-qubit unitaries that these gates decompose.

To understand this structure, for any circuit represented in any gate set, we form maximal 2-qubit unitaries and plot their position within the Weyl chamber, as shown in Figure 13.

The distribution of 2-qubit unitaries drawn from circuits is not random. The input structure of the Adder group is spread out (it contains diverse unitaries), and it so happens that expressive gates, such as B, have trouble representing some of them. On the other hand, the input structure of the QFT algorithm is more periodic which allows Sycamore and B-gates to represent it well.

B. Synthesis Derived Gate Selection Criteria

The incorporation of circuit synthesis in our compilation workflow enables us to derive additional criteria for gate selection and development. The advantages derived from our flow are due to synthesis’ powerful compilation capabilities.

Given an input circuit, traditional compilers will use local peepholes optimizations, translating from one gate set to another using analytical, one-to-one gate rewriting rules for 2-qubit gates. For example, a CNOT is translated into a sequence of two Sycamore gates and additional U3 gates. Any 2-qubit unitary can be represented using at most three CNOT gates.

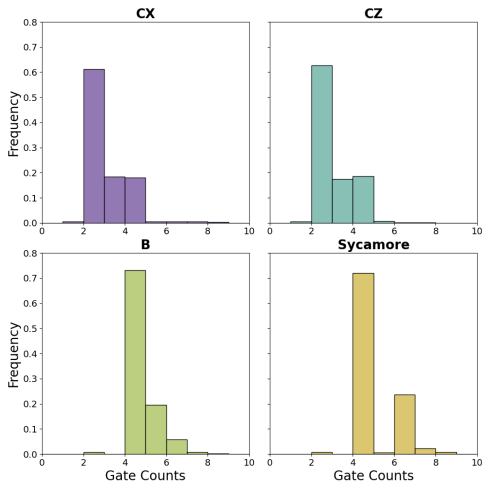


Fig. 15: Gate counts for 3-qubit unitaries present in the input and output circuits of the Hubbard group. The input circuit is the CNOT (top left) graph and the output circuits for each 2-qubit gate set is shown. Unsurprisingly CZ and CNOT have similar distributions, while Sycamore leads to a completely shifted distribution. The B-gate fails to express the simple blocks (fewer than 4 CNOT gates) efficiently but is able to simplify some of the longer blocks.

Thus it is expected to use more Sycamore than CNOT gates to represent an arbitrary 2-qubit gate. As mentioned, it takes at most two B-gates to implement random 2-qubit processes.

One-to-one gate rewriting has been shown to be less than optimal [44]. BQSKit’s synthesis based compiler [45] employs a different strategy. Given an input circuit, BQSKit partitions it into multi-qubit blocks (partitions). Each partition is optimized and translated using optimal topology aware direct unitary synthesis [13], combined with a powerful synthesis based mapping and routing algorithm [26]. Thus, deploying synthesis leads to different conclusions than when using vendor provided compilers, as we see in Figure 14.

More insights can be gained by examining gate representational power to implement 3-qubit blocks/processes that arise in algorithm implementations. We use the BQSKit partitioner to decompose a circuit in maximal 3-qubit gates and then use direct synthesis to generate circuits targeting each native gate set. This procedure results in implementations for each block that use an optimal number of 2-qubit gates, irrespective of gate choice. We plot the gate count distribution of blocks in Figure 15. The CNOT family of gates unsurprisingly have a one-to-one mapping, but the story changes for the Sycamore and B-gates. Using Sycamore gates increases gate count, which is to be expected. On the other hand, we see that the B-gate is able to better express some more complicated blocks (5-7 CNOT blocks reduce to 4 B-gates). However, the overall gate count reduction is held back by the B-gate’s inability to express simpler blocks efficiently. While a larger block granularity (4+ qubits) would not remove all simple blocks from these circuits, it remains to be seen whether the average increased complexity in each block would allow the B-gate to outperform other gates.

Overall, this analysis indicates that existing gate design criteria should be augmented. In addition to choosing a gate

based on attainable fidelity and its representational power for *random* 2-qubit unitaries, the gate representational power for multi-qubit blocks (e.g. three qubit unitaries), drawn from implementations of real workloads, should be considered.

IX. DISCUSSION

While we have introduced and examined several models, we have emphasized the derivation of the roofline approach for the digital fidelity model. A similar derivation can be made for the cyclic model, emphasizing a relative roofline for 1-qubit and 2-qubit process fidelities. Each cycle’s fidelity has an absolute parallelism threshold of $\frac{1}{P_i}$ according to the model, and this number will reduce as specific machines/circuits are targeted. We have also emphasized building a roofline model for hardware improvement by considering relative gate fidelity across two configurations. This derivation is useful to hardware designers and algorithm developers. By changing emphasis from fidelity to gate count and circuit depth, a similar derivation can produce roofline models for compiler developers to guide circuit optimization decisions: “What mix of gates to choose?; “Should I reduce gate count or increase gate parallelism?” etc.

Multiple studies [24], [39] have touched on the idea of co-designing quantum hardware, compilers and algorithms. This paper extends this process by considering device gate sets that target specific algorithms. For TFIM, QFT, and QAE circuits, we have shown that a designer should maximize gate fidelity even at the cost of expressivity and entanglement capability. On the other hand, we see highly expressive gates such as the B-gate provide little improvement in overall circuit fidelity.

We see that restricting the topology from an all-to-all connectivity leads to a potentially massive need for higher gate fidelity, varying by algorithm. This means that for Adder-based circuits, Hubbard models, or QML networks, an ion trap machine with a ZZ or XX gate is best suited.

Our results indicate that unlike classical benchmarking which is compiler independent, quantum system evaluation and benchmarking is sensitive to the quality of compilation tools. For the time being, the compilation workflow requires circuit synthesis for robust inferences.

We believe our methodology will apply beyond the NISQ era into the Fault Tolerant (FT) quantum regime. The model invariant is the circuit gate count. While for NISQ, we directly minimize two-qubit gate count, FT quantum computing requires minimization of error correction overhead, such as non-transversal T gates. Error correction overhead is proportional to the number of one-qubit gates in a circuit and ignores two-qubit gates, leading some circuit decompositions to prioritize single-qubit gate counts [31]. On the other hand, the one-qubit gate count in a circuit is a consequence of the representational power of entangling gates.

X. CONCLUSION

In this paper, we introduce a procedure for performing comparisons between quantum system configurations. In our

quantum roofline analysis, we derive bounds on system properties (e.g. gate fidelity) that can be used as a stop criteria for optimization efforts. We then evaluate machines across a large set of important algorithms and are able to quantify the trade-off required between gate fidelity, expressivity, and entanglement for different circuit families in order to maximize circuit execution fidelity. Our work also shows that the ability of circuit synthesis to generate resource minimal circuits is paramount to performance evaluation, and it enables new design criteria for gate set adoption. We believe our procedure is of interest not only to hardware designers, but compiler and algorithm developers as well.

REFERENCES

- [1] S. Aaronson and L. Chen, “Complexity-Theoretic Foundations of Quantum Supremacy Experiments,” *arXiv:1612.05903 [quant-ph]*, Dec. 2016, arXiv: 1612.05903. [Online]. Available: <http://arxiv.org/abs/1612.05903>
- [2] F. Arute, K. Arya, R. Babbush, D. Bacon, J. C. Bardin, R. Barends, R. Biswas, S. Boixo, F. G. S. L. Brandao, D. A. Buell, B. Burkett, Y. Chen, Z. Chen, B. Chiaro, R. Collins, W. Courtney, A. Dunsworth, E. Farhi, B. Foxen, A. Fowler, C. Gidney, M. Giustina, R. Graff, K. Guerin, S. Habegger, M. P. Harrigan, M. J. Hartmann, A. Ho, M. R. Hoffmann, T. Huang, T. S. Humble, S. V. Isakov, E. Jeffrey, Z. Jiang, D. Kafri, K. Kechedzhi, J. Kelly, P. V. Klimov, S. Knysh, A. N. Korotkov, F. Kostritsa, D. Landhuis, M. Lindmark, E. Lucero, D. Lyakh, S. Mandra, J. R. McClean, M. McEwen, A. Megrant, X. Mi, K. Michielsen, M. Mohseni, J. Mutus, O. Naaman, M. Neeley, C. Neill, M. Y. Niu, E. Ostby, A. Petukhov, J. C. Platt, C. Quintana, E. G. Rieffel, P. Roushan, N. C. Rubin, D. Sank, K. J. Satzinger, V. Smelyanskiy, K. J. Sung, M. D. Trevithick, A. Vainsencher, B. Villalonga, T. White, Z. J. Yao, P. Yeh, A. Zalcman, H. Neven, and J. M. Martinis, “Supplementary information for “Quantum supremacy using a programmable superconducting processor”,” *Nature*, vol. 574, no. 7779, pp. 505–510, Oct. 2019, arXiv:1910.11333 [quant-ph]. [Online]. Available: <http://arxiv.org/abs/1910.11333>
- [3] *Highly Scalable Quantum Computing With Atomic Arrays*, Atom Computing, 2023. [Online]. Available: <https://atom-computing.com/wp-content/uploads/2022/08/Atom-Computing-Atomic-Arrays.pdf>
- [4] F. Bao, H. Deng, D. Ding, R. Gao, X. Gao, C. Huang, X. Jiang, H.-S. Ku, Z. Li, X. Ma, X. Ni, J. Qin, Z. Song, H. Sun, C. Tang, T. Wang, F. Wu, T. Xia, W. Yu, F. Zhang, G. Zhang, X. Zhang, J. Zhou, X. Zhu, Y. Shi, J. Chen, H.-H. Zhao, and C. Deng, “Fluxonium: an alternative qubit platform for high-fidelity operations,” *Physical Review Letters*, vol. 129, no. 1, p. 010502, Jun. 2022, arXiv:2111.13504 [quant-ph]. [Online]. Available: <http://arxiv.org/abs/2111.13504>
- [5] R. Barends, J. Kelly, A. Megrant, D. Sank, E. Jeffrey, Y. Chen, Y. Yin, B. Chiaro, J. Mutus, C. Neill, P. O’Malley, P. Roushan, J. Wenner, T. C. White, A. N. Cleland, and J. M. Martinis, “Coherent josephson qubit suitable for scalable quantum integrated circuits,” *Phys. Rev. Lett.*, vol. 111, p. 080502, Aug 2013. [Online]. Available: <https://link.aps.org/doi/10.1103/PhysRevLett.111.080502>
- [6] S. Beauregard, “Circuit for Shor’s algorithm using $2n+3$ qubits,” Feb. 2003, arXiv:quant-ph/0205095. [Online]. Available: <http://arxiv.org/abs/quant-ph/0205095>
- [7] S. Bravyi and A. Kitaev, “Fermionic quantum computation,” *Annals of Physics*, vol. 298, no. 1, pp. 210–226, May 2002, arXiv:quant-ph/0003137. [Online]. Available: <http://arxiv.org/abs/quant-ph/0003137>
- [8] M. Cerezo, G. Verdon, H.-Y. Huang, L. Cincio, and P. J. Coles, “Challenges and opportunities in quantum machine learning,” *Nature Computational Science*, vol. 2, no. 9, pp. 567–576, Sep. 2022, number: 9 Publisher: Nature Publishing Group. [Online]. Available: <https://www.nature.com/articles/s43588-022-00311-3>
- [9] J.-S. Chen, E. Nielsen, M. Ebert, V. Inlek, K. Wright, V. Chaplin, A. Maksymov, E. Pérez, A. Poudel, P. Maunz, and J. Gamble, “Benchmarking a trapped-ion quantum computer with 29 algorithmic qubits,” Aug. 2023, arXiv:2308.05071 [quant-ph]. [Online]. Available: <http://arxiv.org/abs/2308.05071>
- [10] J. I. Cirac and P. Zoller, “Quantum computations with cold trapped ions,” *Phys. Rev. Lett.*, vol. 74, pp. 4091–4094, May 1995. [Online]. Available: <https://link.aps.org/doi/10.1103/PhysRevLett.74.4091>
- [11] A. Cowtan, S. Dilkes, R. Duncan, W. Simmons, and S. Sivarajah, “Phase gadget synthesis for shallow circuits,” *Electronic Proceedings in Theoretical Computer Science*, vol. 318, p. 213–228, May 2020. [Online]. Available: <http://dx.doi.org/10.4204/EPTCS.318.13>
- [12] A. W. Cross, L. S. Bishop, S. Sheldon, P. D. Nation, and J. M. Gambetta, “Validating quantum computers using randomized model circuits,” *Physical Review A*, vol. 100, no. 3, p. 032328, Sep. 2019, arXiv:1811.12926 [quant-ph]. [Online]. Available: <http://arxiv.org/abs/1811.12926>
- [13] M. G. Davis, E. Smith, A. Tudor, K. Sen, I. Siddiqi, and C. Iancu, “Towards optimal topology aware quantum circuit synthesis,” in *2020 IEEE International Conference on Quantum Computing and Engineering (QCE)*, 2020, pp. 223–234.
- [14] C. Developers, “Cirq,” Jul. 2023. [Online]. Available: <https://doi.org/10.5281/zenodo.8161252>
- [15] A. Erhard, J. J. Wallman, L. Postler, M. Meth, R. Stricker, E. A. Martinez, P. Schindler, T. Monz, J. Emerson, and R. Blatt, “Characterizing large-scale quantum computers via cycle benchmarking,” *Nature Communications*, vol. 10, no. 1, nov 2019. [Online]. Available: <https://doi.org/10.1038/s41467-019-13068-7>
- [16] E. Farhi, J. Goldstone, and S. Gutmann, “A Quantum Approximate Optimization Algorithm,” Nov. 2014, arXiv:1411.4028 [quant-ph]. [Online]. Available: <http://arxiv.org/abs/1411.4028>
- [17] D. Herman, C. Googin, X. Liu, A. Galda, I. Safro, Y. Sun, M. Pistoia, and Y. Alexeev, “A Survey of Quantum Computing for Finance,” Jun. 2022, arXiv:2201.02773 [quant-ph, q-fin]. [Online]. Available: <http://arxiv.org/abs/2201.02773>
- [18] P. Horodecki, M. Horodecki, and R. Horodecki, “General teleportation channel, singlet fraction and quasi-distillation,” Mar. 1999, arXiv:quant-ph/9807091. [Online]. Available: <http://arxiv.org/abs/quant-ph/9807091>
- [19] IonQ Staff, “IonQ Forte: The First Software-Configurable Quantum Computer.” [Online]. Available: <https://ionq.com/resources/ionq-forte-first-configurable-quantum-computer>
- [20] D. Jaksch, J. I. Cirac, P. Zoller, S. L. Rolston, R. Côté, and M. D. Lukin, “Fast quantum gates for neutral atoms,” *Phys. Rev. Lett.*, vol. 85, pp. 2208–2211, Sep 2000. [Online]. Available: <https://link.aps.org/doi/10.1103/PhysRevLett.85.2208>
- [21] Y. Kim, A. Eddins, S. Anand, K. X. Wei, E. van den Berg, S. Rosenblatt, H. Nayfeh, Y. Wu, M. Zaletel, K. Temme, and A. Kandala, “Evidence for the utility of quantum computing before fault tolerance,” *Nature*, vol. 618, no. 7965, pp. 500–505, Jun. 2023, number: 7965 Publisher: Nature Publishing Group. [Online]. Available: <https://www.nature.com/articles/s41586-023-06096-3>
- [22] E. Knill, D. Leibfried, R. Reichle, R. Britton, R. B. Blakestad, J. D. Jost, C. Langer, R. Ozeri, S. Seidelin, and D. J. Wineland, “Randomized Benchmarking of Quantum Gates,” *Physical Review A*, vol. 77, no. 1, p. 012307, Jan. 2008, arXiv:0707.0963 [quant-ph]. [Online]. Available: <http://arxiv.org/abs/0707.0963>
- [23] G. Li, Y. Ding, and Y. Xie, “Tackling the qubit mapping problem for nisq-era quantum devices,” 2019.
- [24] G. Li, A. Wu, Y. Shi, A. Javadi-Abhari, Y. Ding, and Y. Xie, “On the Co-Design of Quantum Software and Hardware,” in *Proceedings of the Eight Annual ACM International Conference on Nanoscale Computing and Communication*, ser. NANOCOM ’21. New York, NY, USA: Association for Computing Machinery, Sep. 2021, pp. 1–7. [Online]. Available: <https://dl.acm.org/doi/10.1145/3477206.3477464>
- [25] S. F. Lin, S. Sussman, C. Duckering, P. S. Mundada, J. M. Baker, R. S. Kumar, A. A. Houck, and F. T. Chong, “Let each quantum bit choose its basis gates,” in *2022 55th IEEE/ACM International Symposium on Microarchitecture (MICRO)*, 2022, pp. 1042–1058.
- [26] J. Liu, E. Younis, M. Weiden, P. Hovland, J. Kubiawicz, and C. Iancu, “Tackling the Qubit Mapping Problem with Permutation-Aware Synthesis,” May 2023, arXiv:2305.02939 [quant-ph]. [Online]. Available: <http://arxiv.org/abs/2305.02939>
- [27] E. Magesan, J. M. Gambetta, and J. Emerson, “Robust randomized benchmarking of quantum processes,” *Physical Review Letters*, vol. 106, no. 18, p. 180504, May 2011, arXiv:1009.3639 [quant-ph]. [Online]. Available: <http://arxiv.org/abs/1009.3639>
- [28] E. Magesan, J. M. Gambetta, and J. Emerson, “Characterizing Quantum Gates via Randomized Benchmarking,” *Physical Review A*, vol. 85,

- no. 4, p. 042311, Apr. 2012, arXiv:1109.6887 [quant-ph]. [Online]. Available: <http://arxiv.org/abs/1109.6887>
- [29] A. Mandviwalla, K. Ohshiro, and B. Ji, "Implementing Grover's Algorithm on the IBM Quantum Computers," in *2018 IEEE International Conference on Big Data (Big Data)*, Dec. 2018, pp. 2531–2537. [Online]. Available: <https://ieeexplore.ieee.org/document/8622457>
- [30] J. R. McClean, I. D. Kivlichan, D. S. Steiger, Y. Cao, E. S. Fried, C. Gidney, T. Häner, V. Havlíček, Z. Jiang, M. Neeley, J. Romero, N. Rubin, N. P. D. Sawaya, K. Setia, S. Sim, W. Sun, K. Sung, and R. Babbush, "Openfermion: The electronic structure package for quantum computers," 2017, cite arxiv:1710.07629. [Online]. Available: <http://arxiv.org/abs/1710.07629>
- [31] M. Möttönen, J. J. Vartiainen, V. Bergholm, and M. M. Salomaa, "Quantum circuits for general multiqubit gates," *Physical review letters*, vol. 93, no. 13, p. 130502, 2004.
- [32] M. A. Nielsen, "A simple formula for the average gate fidelity of a quantum dynamical operation," *Physics Letters A*, vol. 303, no. 4, pp. 249–252, oct 2002. [Online]. Available: <https://doi.org/10.1016%2Fs0375-9601%2802%2901272-0>
- [33] L. B. Oftelie, R. V. Beuemen, E. Younis, E. Smith, C. Iancu, and W. A. de Jong, "Constant-depth circuits for dynamic simulations of materials on quantum computers," *Materials Theory*, vol. 6, no. 1, mar 2022. [Online]. Available: <https://doi.org/10.1186%2Fs41313-022-00043-x>
- [34] A. Peruzzo, J. McClean, P. Shadbolt, M.-H. Yung, X.-Q. Zhou, P. J. Love, A. Aspuru-Guzik, and J. L. O'Brien, "A variational eigenvalue solver on a quantum processor," *Nature Communications*, vol. 5, no. 1, p. 4213, Jul. 2014, arXiv:1304.3061 [physics, physics:quant-ph]. [Online]. Available: <http://arxiv.org/abs/1304.3061>
- [35] Qiskit contributors, "Qiskit: An open-source framework for quantum computing," 2023.
- [36] *Quantinuum System Model H2*, Quantinuum, 2023.
- [37] P. Rakyta and Z. Zimborás, "Efficient quantum gate decomposition via adaptive circuit compression," 2022.
- [38] *Aspen-M-3 Quantum Processor*, Rigetti QCS, 2023.
- [39] H. Safi, K. Wintersperger, and W. Mauerer, "Influence of HW-SW-Co-Design on Quantum Computing Scalability," Jun. 2023, arXiv:2306.04246 [quant-ph]. [Online]. Available: <http://arxiv.org/abs/2306.04246>
- [40] D. Shin, H. Hübener, U. De Giovannini, H. Jin, A. Rubio, and N. Park, "Phonon-driven spin-Floquet magneto-valleytronics in MoS₂," *Nature Communications*, vol. 9, no. 1, p. 638, Feb. 2018, number: 1 Publisher: Nature Publishing Group. [Online]. Available: <https://www.nature.com/articles/s41467-018-02918-5>
- [41] S. Sivarajah, S. Dilkes, A. Cowtan, W. Simmons, A. Edgington, and R. Duncan, "t\$ket\$: A Retargetable Compiler for NISQ Devices," *Quantum Science and Technology*, vol. 6, no. 1, p. 014003, Jan. 2021, arXiv:2003.10611 [quant-ph]. [Online]. Available: <http://arxiv.org/abs/2003.10611>
- [42] R. R. Tucci, "An introduction to cartan's kak decomposition for qc programmers," 2005.
- [43] M. Weiden, E. Younis, J. Kallor, J. Kubiawicz, and C. Iancu, "Improving Quantum Circuit Synthesis with Machine Learning," Jun. 2023, arXiv:2306.05622 [quant-ph]. [Online]. Available: <http://arxiv.org/abs/2306.05622>
- [44] E. Younis and C. Iancu, "Quantum Circuit Optimization and Transpilation via Parameterized Circuit Instantiation," Jun. 2022, arXiv:2206.07885 [quant-ph]. [Online]. Available: <http://arxiv.org/abs/2206.07885>
- [45] E. Younis, C. C. Iancu, W. Lavrijsen, M. Davis, E. Smith, and USDOE, "Berkeley quantum synthesis toolkit (bqskit) v1," 4 2021. [Online]. Available: <https://www.osti.gov/servlets/purl/1785933>
- [46] J. Zhang, J. Vala, S. Sastry, and K. B. Whaley, "Minimum construction of two-qubit quantum operations," *Physical Review Letters*, vol. 93, no. 2, p. 020502, Jul. 2004, arXiv:quant-ph/0312193. [Online]. Available: <http://arxiv.org/abs/quant-ph/0312193>